Comparison of three methods for computing the gravitational attraction of tesseroids at satellite altitude

LONGJUN QIU[1,2] AND ZHAOXI CHEN[2]✉

1   Institute of Geology, Chinese Academy of Geological Sciences, Beijing, China

2   School of Geophysics and Information Technology, China University of Geosciences, Beijing, China (zxchen2010@126.com)

ABSTRACT

Global gravity modelling is one of the most important issues in geophysics and geodesy. Because a tesseroid model comprises the curvature of the Earth, the computation methods for the gravitational potential of tesseroids and its first-order derivatives in spherical coordinates are attracting great attention in recent years. In this paper, we deal with the numerical evaluation of the radial component of the gravitational attraction generated by tesseroid masses at satellite height with the Gauss-Legendre quadrature (GLQ), the Taylor series expansion (TSE) and the prism approximation (PA) methods. Forward modelling of tesseroids of $1° \times 1°$ and $5' \times 5'$ are performed by three computation methods and the comparison between them are made in terms of computational efficiency and accuracy. The numerical results show that the GLQ of order 5 can provide the adequate accuracy for the gravity modelling of $1° \times 1°$ tesseroids at satellite height. The GLQ of order 2 and TSE methods are superior to the PA approach in both computational accuracy and efficiency. The satellite height has important impact on the accuracy of the GLQ and TSE, whereas it has no effect on the PA method. In addition, we developed combined GLQ approach and combined TSE method, respectively, for global gravity modelling based on $1° \times 1°$ and $5' \times 5'$ tesseroids. Apart from the synthetic tesseroids, $1° \times 1°$ data from the CRUST1.0 global crustal model and $5' \times 5'$ rock-equivalent topographic data from the Earth2014 model are used to validate two combined methods. The numerical results show that these two combined methods can balance the computational accuracy and efficiency.

K e y w o r d s : Gauss-Legendre quadrature, tesseroid, Taylor series expansion, comparison

1. INTRODUCTION

The forward modelling of the gravitational attraction of the topographic masses and crustal masses plays a crucial role in geodesy and geophysics. Classical prismatic method provides the closed formulas for the gravitational potential and attraction (*Li and*

Chouteau, 1998; *Nagy et al., 2000, 2002*). However, this method is only applied to the local gravity field investigation because it is related to the planar approximation of the Earth's surface, that is, the effect of the curvature of the Earth is not taken into account. Therefore how to calculate the gravity effect of mass distribution accurately and efficiently is the major issue in the simulation of global gravity field. The key to this problem is to build a model to describe the global mass distribution. A spherical prism called tesseroid, which is bounded by two concentric spheres and the geographic grid, is proved an efficient mass element in global gravity modelling (*Wild-Pfeiffer, 2008*). Because there are no analytical solutions for the gravity modelling of a tesseroid, many researchers have proposed different computational approaches to obtain numerical solutions. *von Frese et al. (1981)* and *Asgharzadeh et al. (2007)* developed the Gauss-Legendre quadrature integration formula for the gravitational effect of a tesseroid based on the equivalent point source. *Uieda et al. (2016)* devised a software Tesseroids to compute the gravitational field by means of the adaptive subdivision of the mass body and the Gauss-Legendre quadrature (GLQ) integration. *Heck and Seitz (2007)* provided an approximate solution of the tesseroid integrals based on Taylor series expansion including third-order terms. *Shen and Deng (2016)* reformulated the higher-order formula including fifth-order terms to obtain more accurate approximation. A tesseroid can be converted into a prism with equivalent mass and its corresponding gravitational effect is achieved by means of the closed formula of the prism while three dimensions of the tesseroid are very small and the distance of the tesseroid to the origin of the geocentric coordinate system is large (*Wild-Pfeiffer, 2008*). The achievement of the prism approximation method needs additional coordinate system transformation (*Heck and Seitz, 2007*). *Marotta and Barzaghi (2017)* devised a methodology to compute the effect of a tesseroid based on the analytical solution of a sector of a spherical zonal band, and this method is compared with the Taylor series expansion (TSE) method by *Marotta et al. (2019)*. *Zhong et al. (2019)* transformed the volume integrals of gravitational signals over a tesseroid into 1D edge integrals and two 2D surface integrals.

In this article, numerical investigations are performed to assess the computational accuracy and efficiency of three methods including prism approximation (PA), GLQ and TSE. We use these three methods to model the vertical component of the gravitational attraction of tesseroids at satellite height. We do not use other special effort like the subdivision of the tesseroid. Considering the impact of the size of tesseroids, all numerical methods are compared based on the experiment settings of $1° × 1°$ and $5′ × 5′$ tesseroids, respectively. In order to balance the computational accuracy and efficiency, the combined GLQ and combined TSE methods are developed and the validations of these two combined methods are tested based on synthetic tesseroids and real crustal model and topographic data sets.

In Section 2.1, we give a brief introduction of the gravitational attraction of a tesseroid. In Section 2.2, we review three computation approaches including GLQ, TSE and PA. In Section 2.3, we propose general computation strategies and describe the combined GLQ and combined TSE methods that are used in this article. In Section 3.1, we analyze the discretization errors, and in Section 3.2 we compare three computation methods by calculating and analyzing the approximation errors produced by these methods based on a homogenous spherical shell. In Section 3.3, we develop two kinds of combined methods (the combined GLQ method and the combined TSE method) to make

the trade-off between the computational accuracy and efficiency. The validation of the two combined methods are tested based on the real model CRUST1.0 global crustal model and the rock-equivalent topography of Earth2014 model, respectively. Finally, we give the conclusions in Section 4.

2. METHODS OF GRAVITY MODELLING FOR A TESSEROID

2.1. The gravitational attraction of a tesseroid

In the present literature contribution, the eccentricity of the Earth tends to be neglected and the spherical approximation provides accurate results in most cases (*Novák and Grafarend, 2005*). Figure 1a shows the geometric parameters of a tesseroid in geocentric coordinate system (x, y, z). If we use (r', φ', λ') and (r, φ, λ) to denote the radius, latitude and longitude of the integration point Q and the computation point P, respectively, the gravitational potential V of a homogenous tesseroid in point P in spherical coordinates can be derived by Newton's integral

$$V(r, \varphi, \lambda) = G\rho \int_{\lambda_1}^{\lambda_2} \int_{\varphi_1}^{\varphi_2} \int_{r_1}^{r_2} \frac{r'^2 \cos\varphi'}{\ell(P, Q)} \, dr' \, d\varphi' \, d\lambda', \tag{1}$$

where G is the gravitational constant and ρ is constant density, r_1 and r_2 are the radii from the top and bottom surfaces of a tesseroid to the center, respectively, λ_1 and λ_2 are western and eastern longitudes, respectively, φ_1 and φ_2 are southern and northern latitudes, respectively, and

$$\ell(P, Q) = |PQ| = \sqrt{r^2 + r'^2 - 2r r' \cos\psi} \tag{2}$$

denotes the Euclidean distance between the computation point P and the integration point Q. The angle ψ between OP and OQ (O being the center of the Earth) is described by

$$\cos\psi = \sin\varphi \sin\varphi' + \cos\varphi \cos\varphi' \cos(\lambda - \lambda'). \tag{3}$$

The first-order derivatives of the gravitational potential can be represented in different coordinates. Here we adopt the local north-oriented frame of the computation point P, where the same point P is the origin and the directions of the base $\mathbf{n}_1$, $\mathbf{n}_2$ and $\mathbf{n}_3$ are, respectively, northward, eastward and upward from the point P (Fig. 1b). The gravitational attraction $\mathbf{a}$ can be derived by the gradient of the gravitational potential

$$\mathbf{a} = \text{grad}\, V = a_i \mathbf{n}_i, \quad i = 1, 2, 3. \tag{4}$$

We mainly deal with the vertical component a_3 of the attraction caused by a tesseroid. The vertical component is expressed as (*Grombein et al., 2013*)
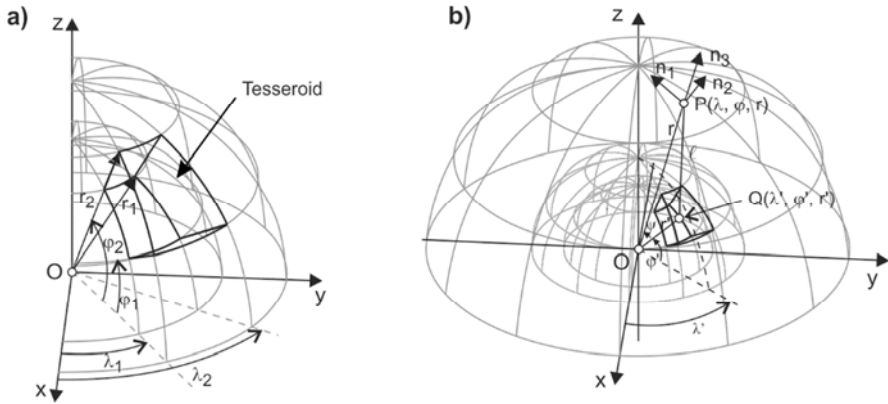
Fig. 1. **a)** The geometry of a tesseroid (solid black) in geocentric coordinates (x, y, z). The point O is the center of the Earth, x axis extends from O to the intersection of the equator and the prime meridian, and z axis is aligned with the rotational axis; r_1 and r_2 are the radii from the top and bottom surfaces of a tesseroid to the center, respectively; λ_1 and λ_2 are western and eastern longitudes, respectively; φ_1 and φ_2 are southern and northern latitudes, respectively; **b)** $\boldsymbol{n}_1$, $\boldsymbol{n}_2$ and $\boldsymbol{n}_3$ are unit vectors of the local north-oriented frame at the computation point P.

$$a_3\left(r, \varphi, \lambda\right) = G\rho \int\limits_{\lambda_1}^{\lambda_2} \int\limits_{\varphi_1}^{\varphi_2} \int\limits_{r_1}^{r_2} \frac{\left(r' \cos\psi - r\right) r'^2 \cos\varphi'}{\ell^3\left(P, Q\right)} \, dr' \, d\varphi' \, d\lambda' . \tag{5}$$

When the computation point P is along the rotation axis of the Earth, an analytical solution for Eq. (5) axists and the closed formula is (*Marotta et al., 2019*)

$$a_3\left(r\right) = \frac{G\rho}{r^2}\left(\lambda_2 - \lambda_1\right)\left(I_2 - I_1\right), \tag{6}$$

where

$$I_1 = \left\{ \frac{1}{3}\left[r'^2 + r^2\left(3\sin^2\varphi_2 - 2\right) + r\,r'\sin\varphi_2\right]\sqrt{r'^2 + r^2 - 2r\,r'\sin\varphi_2}\right.$$
$$\left. + r^3\sin\varphi_2\left(\sin^2\varphi_2 - 1\right)\ln\left[2\left(\sqrt{r'^2 + r^2 - 2r\,r'\sin\varphi_2} + r' - r\sin\varphi_2\right)\right]\right\}\Bigg|_{r'=r_1}^{r'=r_2}, \tag{7a}$$

and

$$I_2 = \left\{ \frac{1}{3}\left[r'^2 + r^2\left(3\sin^2\varphi_1 - 2\right) + r\,r'\sin\varphi_1\right]\sqrt{r'^2 + r^2 - 2r\,r'\sin\varphi_1}\right.$$
$$\left. + r^3\sin\varphi_1\left(\sin^2\varphi_1 - 1\right)\ln\left[2\left(\sqrt{r'^2 + r^2 - 2r\,r'\sin\varphi_1} + r' - r\sin\varphi_1\right)\right]\right\}\Bigg|_{r'=r_1}^{r'=r_2}. \tag{7b}$$

However, there is no general analytical solution for Eq. (5) in other locations and it can be evaluated by numerical methods, such as prism approximation method (Section 2.2.1), GLQ integration (Section 2.2.2) and TSE approach (Section 2.2.3).

2.2. Numerical methods

2.2.1. The rectangular prism approximation approach

A tesseroid can be replaced with equivalent-mass rectangular prism if its size is small enough. i.e. $\sin(\varphi_2 - \varphi_1) \approx (\varphi_2 - \varphi_1)$ and $(r_2 - r_1) \ll r_1$). In this case, the gravitational attraction of the tesseroid can be obtained by means of computing the gravitational contribution of the corresponding rectangular prism. The geometric transformation between the tesseroid and its equivalent-mass prism is shown in Fig. 2a. The components of the gravitational attraction of a rectangular prism, which are computed by the closed formula provided by *Nagy et al. (2000, 2002)*, are described in the edge system (f_1, f_2, f_3) of the prism. The center point T_0 of the prism top surface is the origin of the edge system, and f_1, f_2 and f_3 axes are directed to North, East and radial direction, respectively (see Fig. 2a). The geometric conversion between the tesseroid and the prism can be obtained by

$$\Delta x = \frac{r_1 + r_2}{2}(\varphi_2 - \varphi_1) = \frac{r_1 + r_2}{2}\Delta\varphi, \tag{8a}$$

$$\Delta y = \frac{r_1 + r_2}{2}(\lambda_2 - \lambda_1)\cos\frac{\varphi_1 + \varphi_2}{2} = \frac{r_1 + r_2}{2}\cos\frac{\varphi_1 + \varphi_2}{2}\Delta\lambda, \tag{8b}$$
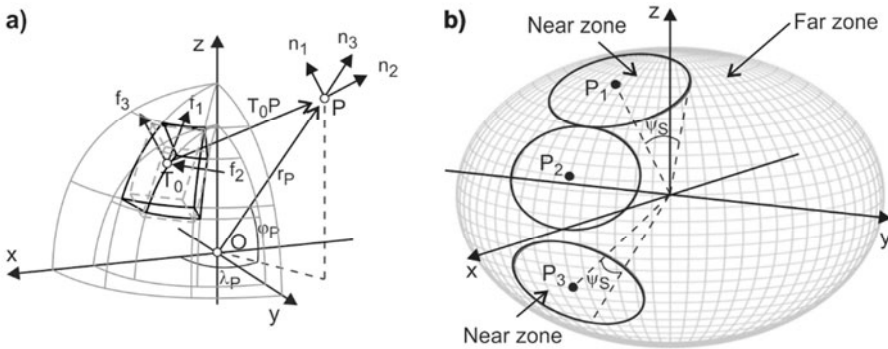
$$\Delta z = r_2 - r_1 = \Delta r, \tag{8c}$$

Fig. 2. **a)** A tesseroid (solid black) and its equivalent-mass rectangular prism (dashed grey); f_1, f_2 and f_3 define the edge system of the rectangular prism with T_0 being its origin. **b)** Scheme of the near zone, the far zone, and the computation points P_1, P_2 and P_3. The area of the near zone can be measured by the central angle ψ_S. The tesseroids in the near zone are different for the same central angle ψ_S.

where Δx, Δy and Δz indicate geometric dimensions of the rectangular prism along $\boldsymbol{f}_1$, $\boldsymbol{f}_2$ and $\boldsymbol{f}_3$, respectively. The deviation between the geometric dimensions of a tesseroid and those of the prism obtained by Eqs (8a)–(8c) will result in inaccurate estimation of the mass when three dimensions of the tesseroid are larger. This improper effect can be corrected by scaling the density of each rectangular prism.

The formulas for the transformation between the edge system of the prism and the global Cartesian coordinate system and the transformation between the local coordinate system of the computation point and global system can be expressed by

$$\left(\boldsymbol{f}_1, \boldsymbol{f}_2, \boldsymbol{f}_3 \right)^{\mathrm{T}} = \mathbf{K}_y \cdot \mathbf{R}_y \left(90 - \varphi_{T_0} \right) \cdot \mathbf{R}_z \left(180 - \lambda_{T_0} \right) \cdot \left(\boldsymbol{e}_x, \boldsymbol{e}_y, \boldsymbol{e}_z \right)^{\mathrm{T}}, \qquad (9a)$$

$$\left(\boldsymbol{n}_1, \boldsymbol{n}_2, \boldsymbol{n}_3 \right)^{\mathrm{T}} = \mathbf{K}_y \cdot \mathbf{R}_y \left(90 - \varphi_P \right) \cdot \mathbf{R}_z \left(180 - \lambda_P \right) \cdot \left(\boldsymbol{e}_x, \boldsymbol{e}_y, \boldsymbol{e}_z \right)^{\mathrm{T}}, \qquad (9b)$$

where λ_{T_0} (φ_{T_0}) and λ_P (φ_P) are the longitude (latitude) of the point T_0 and the computation point P, respectively; $\mathbf{R}_y$ and $\mathbf{R}_z$ denote rotation matrices for rotations of the global Cartesian coordinates clockwise about the y and z axes, respectively; and reflective matrix $\mathbf{K}_y$ reverses the direction of y axis to achieve the transformation of the coordinates; $\boldsymbol{e}_x$, $\boldsymbol{e}_y$ and $\boldsymbol{e}_z$ represent tre base vectors of the global Cartesian coordinate system. Note the order: $\mathbf{R}_z$ operates first, then $\mathbf{R}_y$, and finally $\mathbf{K}_y$. Based on the Eqs (9a) and (9b), the relation between the edge system of the prism and the local coordinate system of the computation point can be obtained by

$$\left(\boldsymbol{n}_1, \boldsymbol{n}_2, \boldsymbol{n}_3 \right)^{\mathrm{T}}$$
$$= \mathbf{K}_y \cdot \mathbf{R}_y \left(90 - \varphi_P \right) \cdot \mathbf{R}_z \left(\lambda_P - \lambda_{T_0} \right) \cdot \mathbf{R}_y \left(\varphi_{T_0} - 90 \right) \cdot \mathbf{K}_y \left(\boldsymbol{f}_1, \boldsymbol{f}_2, \boldsymbol{f}_3 \right)^{\mathrm{T}}. \qquad (10)$$

The explicit forms of the rotation matrices $\mathbf{R}_y$, $\mathbf{R}_z$ and reflective matrix $\mathbf{K}_y$ are available in *Arfken and Weber (2005)*. The geometric deviation between the prism and the tesseroid leads to the approximation error, which is elaborated in Section 3.

2.2.2. The Taylor series expansion method

The approximate solution of Eq. (5) can be obtained by the Taylor series expansion (TSE). To get the maximum efficiency, the geometrical center of the tesseroid, denoted by $Q_0 \left(r_0, \varphi_0, \lambda_0 \right)$, is chosen as Taylor expansion point (*Heck and Seitz, 2007*; *Deng et al., 2016*)

$$r_0 = \frac{r_1 + r_2}{2}, \quad \varphi_0 = \frac{\varphi_1 + \varphi_2}{2}, \quad \lambda_0 = \frac{\lambda_1 + \lambda_2}{2}. \qquad (11)$$

The integral kernel function

$$\frac{\left(r' \cos \psi - r \right) r'^2 \cos \varphi'}{\ell^3 \left(P, Q \right)}$$

in Eq. (5) can be expanded into Taylor series

$$L(r', \varphi', \lambda') = \frac{(r'\cos\psi - r)r'^2 \cos\varphi'}{\ell^3(P,Q)} = \sum_{i,j,k} L_{i,j,k} (r' - r_0)^i (\varphi' - \varphi_0)^j (\lambda' - \lambda_0)^k , \quad (12)$$

where

$$L_{i,j,k} = \frac{1}{i!\,j!\,k!} \left. \frac{\partial^{i+j+k} L(r',\varphi',\lambda')}{\partial r'^i \partial \varphi'^j \partial \lambda'^k} \right|_{r' = r_0,\, \varphi' = \varphi_0,\, \lambda' = \lambda_0} . \quad (13)$$

Using the Eqs (11)–(13), the integral kernel function for the gravitational attraction in Eq. (5) can be expanded in any order Taylor series expansion. The more accurate approximation needs to select the higher order expansion.

In this article, the expansion with second-order term is used and Eq. (5) can be expressed as

$$a_3 = G\rho\Delta r\Delta\varphi\Delta\lambda \left[L_{000} + \frac{1}{24}\left(L_{200}\Delta r^2 + L_{020}\Delta\varphi^2 + L_{002}\Delta\lambda^2 \right) + O\left(\Delta^4\right) \right], \quad (14)$$

where the Landau symbol $O\left(\Delta^4\right)$ indicates that the omitted Taylor residual has a magnitude of fourth order in Δr, $\Delta\varphi$, $\Delta\lambda$, and the explicit expressions of the coefficients L_{000}, L_{200}, L_{020} and L_{002} are available in *Heck and Seitz (2007)*. The zero-order approximation in Eq. (14) is the gravitational attraction due to a point-mass $m_0 = \rho r_0^2 \cos\phi_0 \Delta r\Delta\varphi\Delta\lambda$ located at the geocentric point Q_0 of the tesseroid. Hence, the formula of the vertical gravitational attraction due to a point-mass is represented as

$$a_3^{pointmass} = G\rho \,\Delta r\Delta\varphi\Delta\lambda L_{000}\left(1 + O\left(\Delta^2\right)\right) = \frac{Gm_0\left(r_0\cos\psi_0 - r\right)}{\ell_0^3}, \quad (15)$$

where

$$\ell_0 = |PQ_0| = \sqrt{r^2 + r'^2 - 2r\,r_0\cos\psi_0} , \quad (16a)$$

$$\cos\psi_0 = \sin\varphi\sin\varphi_0 + \cos\varphi\cos\varphi_0\cos\left(\lambda - \lambda_0\right). \quad (16b)$$

2.2.3. The Gauss-Legendre quadrature integration

The numerical integration by using GLQ formula provided by *Asgharzadeh et al. (2007)* for Eq. (5) can be expressed as

$$\begin{aligned}
a_3(r,\varphi,\lambda) &= G\rho \int_{\lambda_1}^{\lambda_2} \int_{\varphi_1}^{\varphi_2} \int_{r_1}^{r_2} L(r',\varphi',\lambda')\,\mathrm{d}r'\,\mathrm{d}\varphi'\,\mathrm{d}\lambda' \\
&= \frac{\Delta\lambda\,\Delta\varphi\,\Delta r}{8} \sum_{i=1}^{N_\lambda} \sum_{j=1}^{N_\varphi} \sum_{k=1}^{N_r} \omega_{\lambda i}\omega_{\varphi j}\omega_{rk} L\left(r'_k,\varphi'_j,\lambda'_i\right),
\end{aligned} \quad (17)$$

where $L(r', \varphi', \lambda')$ is the integral kernel of the gravitational attraction; N_λ, N_φ and N_r are the integration orders, which determine the number of Gaussian nodes; $\omega_{\lambda i}$, $\omega_{\varphi j}$ and ω_{rk} are the weights of the nodes; r'_k, φ'_j and λ'_i are the radius, latitude and longitude of the nodes; and $L(r'_k, \varphi'_j, \lambda'_i)$ is the evaluation of kernel function at nodes.

The procedure contains two steps, firstly evaluating the values of the kernel function at the specific nodes and then summing the weighted functional values (*von Frese et al., 1981*). Hence, the gravitational attraction due to a source volume can be considered as the sum of the weighted gravitational effect of a number of equivalent point sources (*Ku, 1977*). The numerical accuracy of gravity modelling based on GLQ method depends on the number of the nodes, which means the only concern in applying Eq. (17) is the selection of the nodes. A larger number of nodes will provide accurate numerical solution, however, will consume significantly more computation time. Generally, the uniform nodes are adopted for all the tesseroids, e.g., the integration orders $N_\lambda = 8$, $N_\varphi = 8$, and $N_r = 2$ are used for the gravity modelling in *Asgharzadeh et al. (2007)*, and the orders $N_\lambda = 3$, $N_\varphi = 3$, and $N_r = 2$ in *Roussel et al., (2015)*. The selection for the number of the orders mainly relies on the size of the tesseorid, the computation height and the required accuracy level for the specific application.

2.3. Combined methods for the gravity modelling in space domain

For the global gravity modelling in the case of geodesy applications, the gravitational attraction of the masses in the vicinity of the computation point only makes up a part of the whole effect. The accuracy of the forward modelling of these masses has significant impact on the modelling results, and the gravitational effect of the masses in remote area is filtered due to the fast attenuation character. However, the cumulative contribution of these individual mass bodies in the remote area plays a crucial role in the result due to the superposed impact of a large proportion of the mass bodies (*Tsoulis et al., 2009*). To perform the proper gravity modelling at the Earth's surface, the computation region is divided into different zones with various radii and the different mass elements are used to approximate the real masses in different zones. For instance, *Yang et al. (2020)* divided the whole mass distribution into four zones, and four mass elements including polyhedron, prism, tesseroid and point-mass are used to approximate the real mass. In the case of approximating the real Earth's surface by prisms, the upper boundary of the prismatic elements can be represented by polyhedral tops or bilinear surface. The difference due to the refinement of the top surface is impacted by the original resolution and the height of the gridded data (*Smith et al., 2001*).

Tesseroid mass body is an efficient mass element and it takes the curvature of the Earth into consideration compared with a rectangular prism. The numerical accuracy of the gravity modelling of a tesseroid is impacted by some factors like the size of the tesseroid, the gravity field component (gravitational potential, components of gravitational attraction and components of gravity gradient tensor) to be computed, and the distance between the tesseroid and the computation point (*Roussel et al., 2015*). Among these factors, the distance between the source and the computation point are the most important

issue. When the computation height is small and the tesseroid is closer to the computation point, the approximation errors produced by computation methods increase, and this is called the very near-zone problem (*Shen and Deng, 2016*). To solve this problem, *Heck and Seitz (2007)* believed that the effect of the mass elements in the vicinity of the computation point should be evaluated using the closed formula of a prism. Another alternative solution is to combine the numerical methods with the subdivision technique, which results in the reducing of the errors by dividing the tesseroid into smaller ones. The subdivision includes a regular subdivision (*Grombein et al., 2013*) and an adaptive subdivision (*Li et al., 2011*; *Uieda et al., 2016*; *Lin and Denker, 2019*). When combining the GLQ integration with the adaptive subdivision (GLQ_AD), the number of the GLQ nodes is fixed at relatively small value and a scalar parameter called distance-to-size ratio (*D*) controls the subdivision procedure and affects the approximation error (*Uieda et al., 2016*). Higher value of *D* is needed for the modelling of the high-order derivatives of the gravitational potential (*Deng and Shen, 2019*). Compared with 3D adaptive subdivision, the combination of 3D GLQ integration with 2D adaptive technique proved to be more effective for the improvement of the accuracy (*Lin and Denker, 2019*). Apart from different numerical methods, the computational efficiency can be obtained by the combined use of gridded data with different resolutions, due to the attenuation of the gravitational attraction with distance-squared variation (*Kuhn et al., 2009*).

We use precise numerical formula for tesseroids in the near zone and use a rough and fast method in the far zone. Please note that the combined method can be implemented in different ways and choosing the methods and the relevant parameters should be based on the obtained experience from the previous researches. In the near zone, mass distributions cover a circular area around the computation point and the rest part of mass distributions is in the far zone, which is shown in Fig. 2b. The central angle, formed by the computation point and any point on the boundary between the near zone and far zone, can be used to measure the area of the near zone. Whether the tesseroid is located in the near zone can be determined by this central angle ψ_S. If the spherical distance between the computation point and the geometric center of a tesseroid is less than the given parameter ψ_S, the tesseroid is seen as a mass body in the near zone with respect to this computation point. Figure 2b shows that the number of tesseroids in different near zones and the geometric dimensions of these tesseroids are different for the same parameter ψ_S because the latitude of the computation points changes. This means that the result of the forward modeling is mainly affected by the location of the computation point for the given parameter ψ_S, and the relation between the modeling accuracy and the latitude of the computation point will be shown by the numerical tests in Section 3.3. When it comes to the combined method, the selection of computation methods is related to the specific applications. This paper concerns the GLQ, TSE and PA approaches, in which the GLQ is a flexible approach and can be used for the modeling of tesseroid of $1° \times 1°$ or larger size. When the computation height is at satellite altitude, the integration order 5 is enough for the GLQ approach to obtain the accuracy of 10^{-6} m Gal for the gravity modeling of tesseroid of $1° \times 1°$ (see Section 3.2). Hence, we use the GLQ of order 5 in the near zone and the GLQ of order 2 in the far zone, which is called the combined GLQ method. Although the GLQ of order 5 is more accurate than that of order 2, the computation time of the former is eight times as much as that of the latter (see Section 3.2). The parameter

ψ_S plays an important role in controlling the computation accuracy and computation speed for the combined GLQ method. *Grombein et al. (2010)* used similar combined method to model topographic effect in gravity gradients when the computation point is situated in satellite height, and they suggested ψ_S should be larger than 11° in order to obtained adequate level of accuracy. The larger ψ_S is, the more accurate the forward modeling of the combined GLQ method is. Meantime, the level of accuracy does not significantly change with the area of the near zone. In order to avoid extra computation cost, the excessively big value for ψ_S is unnecessary. We do not perform the forward modeling with every possible value for ψ_S, and we only have carried out the numerical tests for the gravitational attraction using the combined method with $\psi_S = 5°$, 10°, 15° and 20°. In the cases of modelling of the $5' \times 5'$ tesseroids, we use the TSE with second-order term to model the gravitational attraction of the tesseroids in the near zone and TSE with zero-order term in the far zone in order to save computation cost considering the required computation time is increased significantly due to the use of grid resolution of $5' \times 5'$.

3. NUMERICAL TESTS

For all numerical tests in this section, we define the Newton's gravitational constant $G = 6.67191 \times 10^{-11}$ m³ kg⁻¹ s⁻², and the mean radius of the Earth $R_{mean} = 6\ 378\ 137$ m. We set the quadrature orders N_λ, N_φ and N_r along three dimensions to the same value N_{ord}. In the following numerical tests, the GLQ with $N_{ord} = 2$ and 5 are used, and for the sake of conciseness, GLQ method of order 2 and 5 are denoted by GLQ_N2 and GLQ_N5, respectively. All the tests are performed on a Dell workstation T630, which is equipped with two Intel Xeon E5 @ 2.6 GHz CPUs. The computation time shown in Figs 7b and 9b is the parallel computing time. All the codes run based on MATLAB 2019 and Windows 10.

3.1. Algebraic error produced by summation of gravitational impacts of discretized tesseroids

The vertical component of the gravitational attraction of a homogenous spherical shell with the density ρ_s and the thickness Δh at the computation point $P(r_P, \varphi, \lambda)$ is expressed as

$$a_3^{shell} = \frac{4}{3}\pi G \rho_s \left(r_2^3 - r_1^3 \right) \frac{1}{r_P^2}, \quad r_P \geq r_2 \geq r_1, \tag{18}$$

where r_1 and r_2 are the inner and outer radii, respectively, i.e., $r_1 = R_{mean}$ and $r_2 = R_{mean} + \Delta h$, respectively; $r_P = R_{mean} + h_P$, with h_P being the computation height above the surface of the Earth. The spherical symmetry allows us to calculate the gravitational field of the shell at any external computation point using Eq. (18). When the computation point is located at the rotation axis of the Earth, the gravitational contribution of an individual tesseroid can be calculated by Eqs (6), (7a) and (7b). The gravitational field of the shell is also obtained by superposing the impacts of all discretized tesseroids.

Table 1. The algebraic errors $\Delta a_3^{shell-tess}$ for different tesseroid sizes and computation heights h_P.

h_P [km]	Tesseroid size		
	$1' \times 1'$	$5' \times 5'$	$1° \times 1°$
200	3.620×10^{-8}	2.582×10^{-9}	5.002×10^{-11}
400	1.289×10^{-8}	1.092×10^{-9}	1.248×10^{-11}
600	1.563×10^{-8}	-5.920×10^{-9}	1.100×10^{-10}

In the process of superposing the impacts of all tesseroids over the spherical shell, there exists algebraic error in the summation, and its magnitude is related with the number of the discretized tesseroids. In the numerical test, we analyze the relation between the algebraic error and the number of the tesseroids by dividing the spherical shell into 233 280 000 $1' \times 1'$, 9 331 200 $5' \times 5'$, and 64 800 $1° \times 1°$ tesseroids, respectively. We use $\Delta a_3^{shell-tess}$ to indicate the difference between the gravitational contribution of a homogeneous spherical shell obtained by Eq. (18) and the gravitational contribution obtained after the decomposition of the shell into a discrete number of tesseroids and the summation of the single impacts calculated by Eqs (6), (7a) and (7b). The computation heights are set to $h_P = 200$, 400, and 600 km. The results are shown in Table 1 for the case of $\Delta h = 10$ km and the $\rho_s = 2670$ kg m^{-3}. Table 1 shows that $\Delta a_3^{shell-tess}$ has a close correlation with the grid resolution of tesseroids. When the grid resolution or tesseroid size gets smaller, the number of the tesseroids over the shell increases and the magnitude of the algebraic error gets larger. Meantime, it can be seen that there is not an obvious correlation between the computation heigh and the magnitude of the algebraic error for the same grid resolution.

3.2. Comparison of the computation methods in the case of spherical shell

In the following tests, the vertical gravitational attraction of the spherical shell with a thickness of 2 km and a constant density of 2670 kg m^{-3} is chosen as a reference value. We only use the $5' \times 5'$ and $1° \times 1°$ tesseroids to make comparison between three computational methods (GLQ, TSE and PA). The horizontal dimensions of the discretized tesseroids are $1°$ and $5'$, i.e., $\Delta_{tess} = \Delta\lambda = \Delta\varphi = \{1°, 5'\}$. The computation points are located along the meridian 0.25'E from the 0°N to the 90°N, with a spacing of 0.25°, resulting in 361 samples. The computation heights $h_P = 200$, 400 and 600 km have been tested. The shell field at different computation heights can be exactly computed through Eq. (18).

In test 1, Fig. 3 shows the approximation error δa_3 computed by GLQ_N2, GLQ_N5, TSE and PA methods at three different h_P values of 200, 400 and 600 km. The x axis means the latitude of the computation points, which ranges from 0° to 90° with the
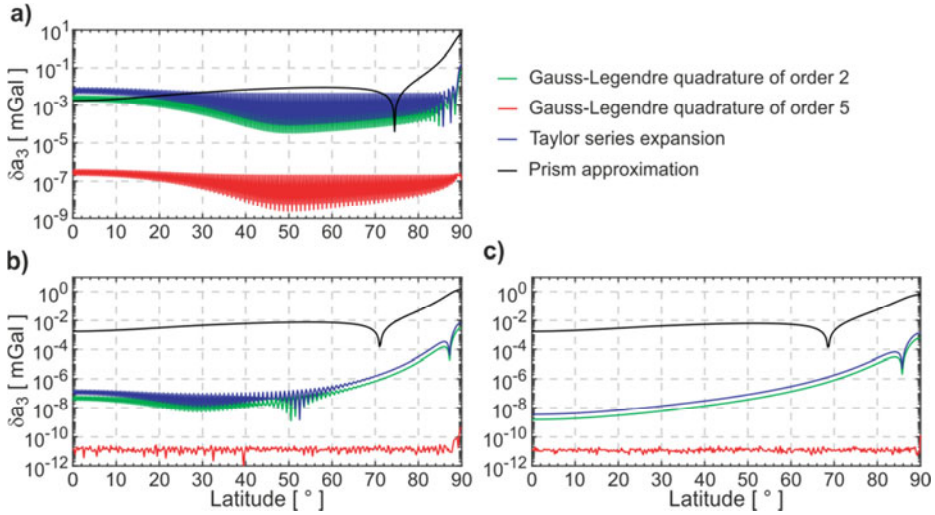
Fig. 3. Approximation error δa_3 of the gravitational attraction of $1° \times 1°$ tesseroids as a function of latitude of the computation point, determined by different methods at three computation heights: **a)** 200, **b)** 400 and **c)** 600 km.

interval of 0.25°. The y axis shows the approximation errors (absolute errors in mGal). It can be seen in Fig. 3 that for the satellite height, the GLQ_N5 method gives the most accurate results compared with GLQ_N2, TSE and PA, but takes more computation time (see Fig. 4). The computation height has significant effect on the accuracy for all methods, and with increasing height, the approximation errors for all methods decrease to different degrees. Because the GLQ_N5 ensures the approximation errors below 10^{-6} and 10^{-10}mGal for 200 and 400 km, respectively, the GLQ integration of order 5 is enough in terms of the accuracy of the gravitational attraction modelling in the case of satellite height. Figure 4 shows the computation time of the GLQ_N5 increases by a factor of eight compared with the GLQ_N2. It means the computation time required by the GLQ grows significantly with increasing order.

It is interesting to note that the trends of two curves for GLQ_N2 and TSE are nearly the same: for $h_P = 200$ km the approximation error curves of these two methods spread within a band that widens at about the latitude 50°N; the dispersion phenomena begins to disappear with the increase of the computation height. On the whole, compared with TSE approach, the GLQ_N2 is a bit more accurate and efficient method.

There is no dispersion characteristics on approximation error curve of the PA method. The difference of the approximation errors between PA method and the TSE method enlarges with the increase of the computation height. The approximation error curve of the PA method remains nearly in the same order magnitude for different computation heights.

The approximation error of PA method mainly results from the difference in the geometric size between the rectangular prism and tesseroid, although the density has been scaled to counterbalance this geometric deviation. The PA method requires about four
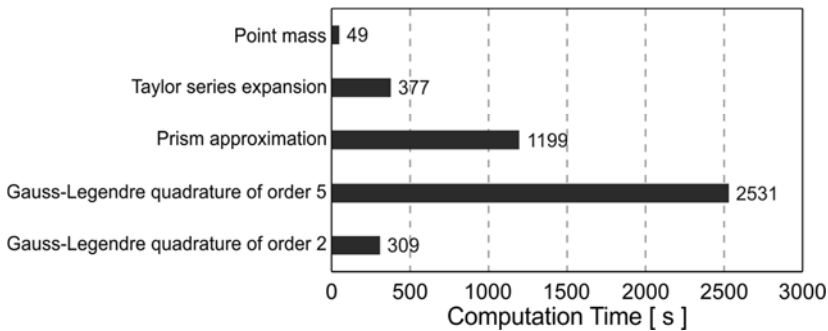
Fig. 4. Computation time for different computational methods in the test 1.

times the computation time of the GLQ_N2, due to the fact that its computation procedure involves several logarithmic and inverse trigonometric functions and additional coordinate transformations.

In test 2, the shell is discretized into individual tesseroids by regular grid with resolution of 5′. The approximation errors caused by GLQ, TSE and PA methods are shown in Fig. 5. Comparing the approximation error curves of GLQ_N5, GLQ_N2, TSE and PA in test 1 with those at the same computation height in test 2, we can see that the errors of GLQ_N2 and TSE decrease obviously because of the reduction of the tesseroid volume. The accuracy of the PA method is increased by about two orders of magnitude due to the fact the geometric deviation between the tesseroid and rectangular prism becomes small. Hence, the PA method is suitable to model the gravitational effect of the small size tesseroids at a low computation height. For the computing gravitational
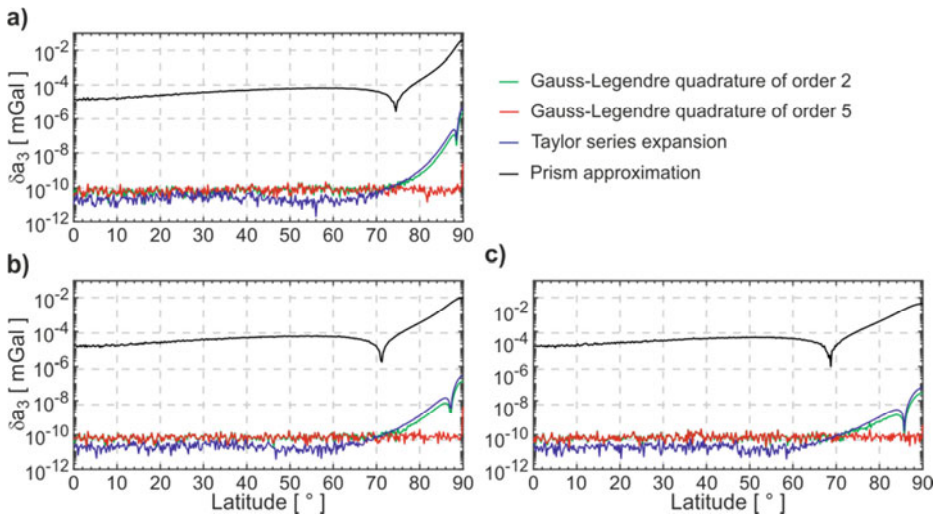

Fig. 5. The same as in Fig. 3, but for the 5′ × 5′ tesseroids.

attraction of $5' \times 5'$ tesseroids at satellite height, the TSE method is preferred, because when the latitude is less than 70°N, it is more accurate than GLQ_N5. Although the errors increase when the latitude is larger than 70°N, the maximum errors caused by GLQ_N2 and TSE methods are only on the order 10^{-5} mGal.

3.3. Numerical tests of the combined method

3.3.1. The case of the modelling of tesseroids of $1° \times 1°$

Considering the GLQ_N5 method provides the accurate result for the $1° \times 1°$ tesseroid, we perform the modelling of the tesseroids by using the GLQ_N5 and GLQ_N2 to calculate the effect of tesseroids in near and far zone, respectively. The $1° \times 1°$ tesseroids are from the discretization of a homogenous spherical shell 2 km thick, with density of 2670 kg m^{-3}. The boundary between the near and far zone is determined by the parameter ψ_S that is mentioned and defined in Section 2.3. The combined GLQ with the parameter ψ_S of 5°, 10°, 15° and 20° are used to calculate the gravitational attraction of 64800 $1° \times 1°$ tesseroids at heights of 200 and 600 km. We also visualize the approximation errors of GLQ_N2 in order to make comparison between the GLQ_N2 and the combined GLQ method. Figure 6a shows that the approximation error of the combined GLQ method is significantly lower than that of GLQ_N2 for the computation height of 200 km, and moreover, the combined GLQ has better numerical stability.

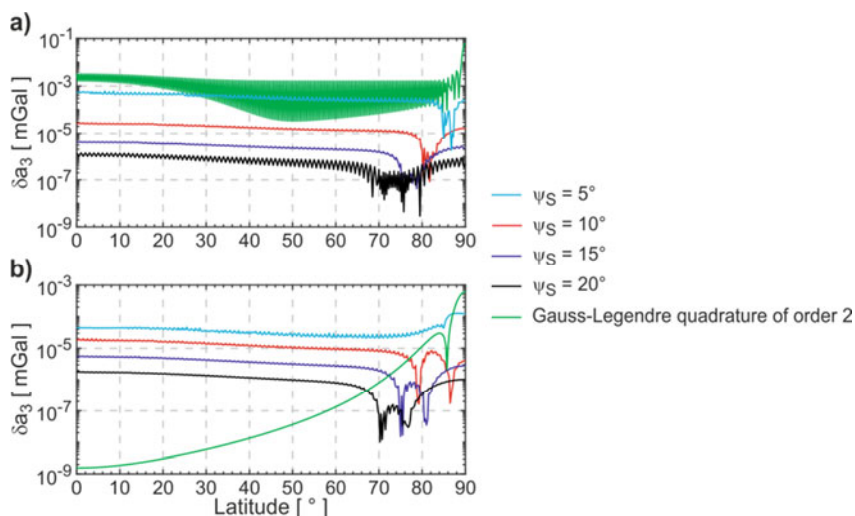For the computation height $h_P = 600$ km, the approximation error of the GLQ_N2

Fig. 6. The approximation error δa_3 of the gravitational attraction of $1° \times 1°$ tesseroids as a function of latitude of the computation point, determined using the Gauss-Legendre quadrature method of order 2 and the combined Gauss-Legendre quadrature method with different values of central angle ψ_S at two computation heights: **a)** 200, **b)** 600 km.

varies with latitude, and it strongly increases from about 10^{-8} mGal at the equator to 10^{-3} mGal at the North Pole. By contrast with GLQ_N2 method, the combined GLQ makes the approximation error more or less constant with varying latitude, and it solves the problem that the approximation error increases significantly when the computation point approaches the North Pole. The GLQ_N2 is a preferred method for the computation height of 600 km if the maximum tolerated error is 10^{-3} mGal.

The numerical test above is based on a homogenous shell and the approximation error produced by individual tesseroid on one computation point can cancel out because of the spherical symmetry. In the following, we use multilayer model CRUST1.0 to test the validation of the combined GLQ method. The $1° \times 1°$ cell of the CRUST1.0 contains boundary depths of the eight layers (water, ice, three sediment layers and upper, middle and lower crystalline crust) and corresponding density as well se seismic velocity (*Laske et al., 2013*). This global curst model has 321 975 cells of nonzero thickness, and the maximum and minimum thickness of these cells is 40 000 and 10 m, respectively. Figure 7a shows the vertical gravitational attraction of the $1° \times 1°$ tesseroids from the
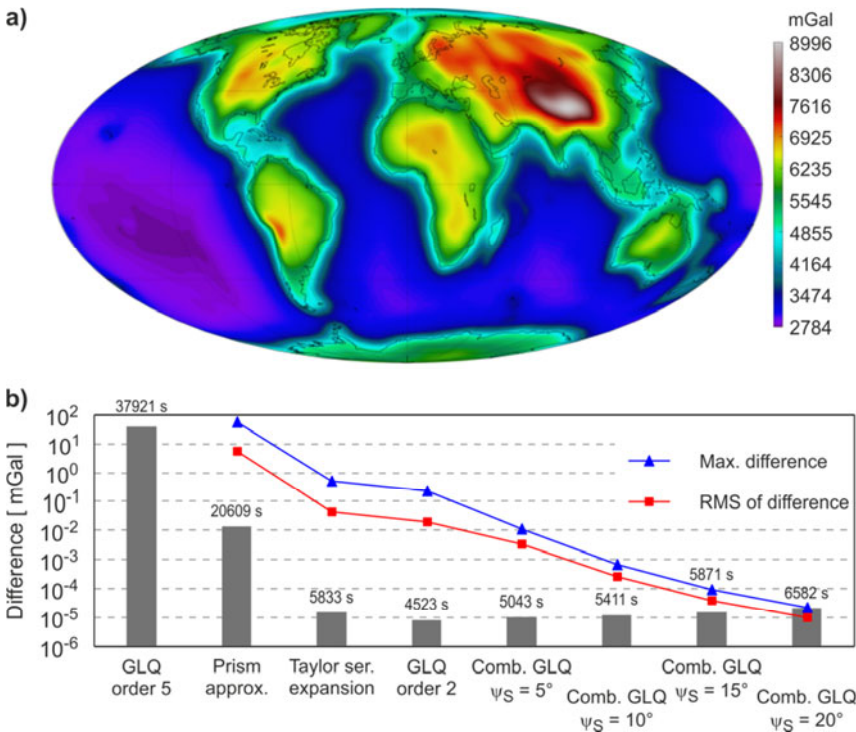

Fig. 7. **a)** Gravitational attraction of the CRUST1.0 model at 255 km using the Gauss-Legendre quadrature (GLQ) of order 5; **b)** Maximum and root-mean-square (*RMS*) differences between the modeling results shown in a) and those obtained by other methods. The computation time is indicated by columns; ψ_S – central angle.

CRUST1.0 at 255 km by means of the GLQ_N5 method. The plot is made using the software provided by *Bezděk and Sebera (2013)*. We also use GLQ_N2, TSE, PA, and the combined GLQ with the parameter ψ_S of 5°, 10°, 15° and 20° to perform the forward modelling. We regard the computed gravity field by the GLQ_N5 as the reference field in order to make comparison between these different numerical solutions. The statistics of results (the maximum and rooted mean square differences) and computation time for all methods mentioned are shown in Fig. 7b.

Compared with the combined GLQ method, the GLQ_N2, TSE and PA methods will produce larger approximation errors. The maximum and root-mean-square (*RMS*) difference between PA and GLQ_N5 are even larger than 50 and 5 mGal, respectively. The PA method also requires more computation time than TSE, GLQ_N2 and the combined GLQ method. The maximum difference and RMS difference of GLQ_N2 are about on the same order magnitude as those of TSE. The combined GLQ makes possible to balance the modelling accuracy and the computation time by choosing the parameter ψ_S. The computation time of the combined GLQ with ψ_S of 5°, 10°, 15° and 20° is only 13.3%, 14.3%, 15.5% and 17.4%, respectively, with respect to the time of GLQ_N5. The combined GLQ with the parameters ψ_S of 10° and 15° makes the maximum difference below 10^{-3} and 10^{-4} mGal, respectively. Compared the case of the spherical shell of 2 km, the absolute error of the combined GLQ method in the case of the CRUST 1.0 increases by a factor of 10.

3.3.2. The case of the modelling of tesseroids of 5′ × 5′

When evaluating the gravitational attraction due to the topographic masses at a satellite height, the computation time is one major concern due to the fact that the Earth's topography is given by a digital terrain model with the resolution of 5′ × 5′ or higher. Because the TSE with second-order term can provides the accuracy level of 10^{-5} mGal at satellite height, which is mentioned in Section 3.2, we can combine the TSE method with second-order term and that with zero-order term to calculate the effect of tesseroids of 5′ × 5′ grid resolution. For the tesseroids in the near zone with respect to the computation point, the TSE with second-order term is used to guarantee calculation accuracy, and for the tesseorids in the far zone, the fastest method TSE with zero-order term is used to obtain the computation efficiency.

We perform the forward modelling of the gravitational attraction of 9 331 200 tesseroids of 5′ × 5′ × 2 km by means of the combined TSE with ψ_S of 5°, 10°, 15° and 20° at 200 and 600 km. The combined TSE method is not affected by the computation height and the approximation errors at 200 and 600 km are almost at the same order magnitude (Fig. 8). In addition, the approximation error of the combined TSE method does not increase when the computation point approaches to the north pole. The combined TSE with $\psi_S = 10°$ makes the errors below 10^{-3} mGal at the altitude of 200 and 600 km.

Apart from the synthetic tesseroids, the 5′ × 5′ topography model is used in the following test. The topographic data is from the Earth2014, which can provide 1′ × 1′ elevations over land, the seafloor or lake-bottom topography and sub-ice topography (*Hirt and Rexer, 2015*). In order to simplify the calculation, we only use 5′ × 5′ rock-equivalent topography with the constant density of 2670 kg m^{-3} to test the validation of the
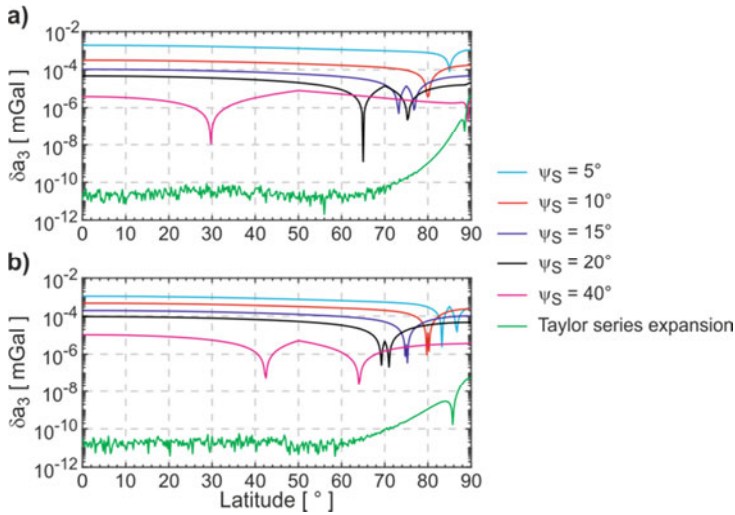
Fig. 8. The same as in Fig. 6, but for the $5' \times 5'$ tesseroids and combined Taylor series expansion.

combined TSE. The reference surface of the topographic data is mean sea level. The ranges of the computation grid are $(135\sim60°)$W and $(0\sim60°)$N and it consists of 150×120 points with a spacing of $0.5°$. We perform the calculation of the gravitational attraction based on the $5' \times 5'$ the rock-equivalent topography by using PA, TSE, GLQ_N2 and the combined TSE with ψ_S of $5°$, $10°$, $15°$ and $20°$ at height of 250 km.

The vertical gravitational attraction of the topographic masses is shown in Fig. 9a. It can be seen that the result is generally characterized by negative anomalies due to the mass deficiency of the ocean area. The computed results of the Great Plains are from -50 to -150 mGal and the maximum value is ~23.9 mGal. The gravitational attraction obtained by TSE with second-order term is regarded as the reference value. The maximum and *RMS* differences between this reference value and the computed results by other numerical methods including PA, GLQ_N2 and the combined TSE with ψ_S of $5°$, $10°$, $15°$ and $20°$ are shown in Fig. 9c. Figure 9c also shows the computation time required by these methods. The PA method costs the most computation time in all methods of this test. The GLQ_N2 and TSE with second-order term consume more computation time than the combined TSE method. The combined TSE with $\psi_S = 10°$ requires only 17.87% of the computation time of the TSE with second-order term and makes the maximum difference below 10^{-3} mGal at satellite altitude.

4. CONCLUSIONS

In this study, we carry out a comparison among the Gauss-Legendre quadrature (GLQ), Taylor series expansion (TSE) and prism approximation approach (PA) that are used for global gravity modelling of tesseroids at satellite height in the view of
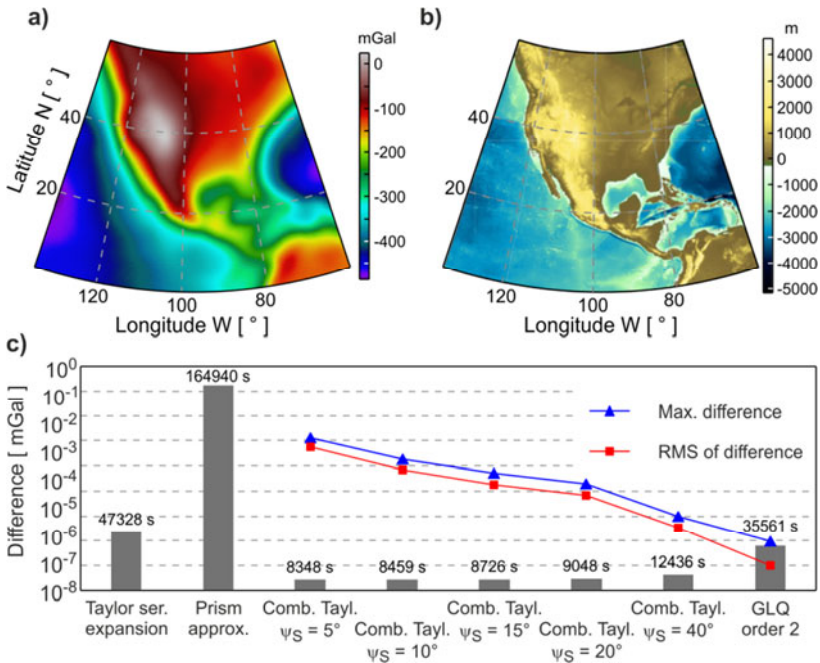
Fig. 9. **a)** The gravitational attraction of the rock-equivalent topography using the Taylor series expansion with second-order term; **b)** the rock-equivalent topography over the computation area; **c)** The maximum and root-mean-square (*RMS*) differences between the modelling results shown in a) and those by other numerical methods. The computation time is indicated by columns; ψ_S – central angle.

computational accuracy and efficiency. In terms of the computational accuracy, three methods have the relation of GLQ > TSE > PA. The approximation error induced by PA method is hardly impacted by the computation height. The GLQ of order 5 (GLQ_N5) can provide the adequate accuracy level for the global gravity modelling of $1° \times 1°$ tesseroids. The computational accuracy of the GLQ of order 2 (GLQ_N2) is almost the same as that of the TSE method, although the latter costs more computational time.

We develop the combined GLQ method and the combined TSE approach to perform the modelling of the gravitational attraction for tesseroids of $1° \times 1°$ and the tesseroids of $5′ \times 5′$, respectively. Central angle ψ_S (in degrees) from the computation point to the geometric center of the tesseroid is used to divide the model domain into the near and far zones. We employ GLQ_N5 in the near zone but GLQ_N2 in the far zone in the combined GLQ method, and analogously we employ TSE with second-order term in the near zone but that with zero-order term in the far zone in the combined TSE method. Two cases of the global gravity modelling based on the CRUST1.0 global crustal model and Earth2014 rock-equivalent topography model are used to test the validation of the two combined methods.

The numerical investigations show that the combined methods provide a reasonable trade-off between the computational accuracy and speed by changing ψ_S. The combined GLQ costs about 18% of the computation time required by GLQ_N5 and the combined TSE costs about 14% of the computation time required by TSE with second-order term in order to obtain the adequate modelling accuracy of 10^{-3} mGal.

References

Arfken G.B. and Weber H.J., 2005. *Mathematical Methods for Physicists*. Sixth Edition. Elsevier - Academic Press, Burlington, MA

Asgharzadeh M.F., von Frese R.R.B., Kim H.R., Leftwich T.E. and Kim J.W., 2007. Spherical prism gravity effects by Gauss-Legendre quadrature integration. *Geophys. J. Int.*, **169**, 1–11

Bezděk A. and Sebera J., 2013. Matlab script for 3D visualizing geodata on a rotating globe. *Comput. Geosci.*, **56**, 127–130

Deng X.L., Grombein T., Shen W.B., Heck B. and Seitz K., 2016. Corrections to "A comparison of the tesseroid, prism and point-mass approaches for mass reductions in gravity field modelling" (Heck and Seitz, 2007) and "Optimized formulas for the gravitational field of a tesseroid" (Grombein et al., 2013). *J. Geodesy*, **90**, 585–587

Deng X.L. and Shen W.B., 2019. Topographic effects up to gravitational curvatures of tesseroids: A case study in China. *Stud. Geophys. Geod.*, **63**, 345–366, DOI: 10.1007/s11200-018-0772-4

Grombein T., Seitz K. and Heck B., 2010. Modelling topographic effects in GOCE gravity gradients. In: Münch U. and Dransch W. (Eds), *Geotechnologien Science Report*, **17**, 84–93, DOI: 10.2312/GFZ.gt.17.13

Grombein T., Seitz K. and Heck B., 2013. Optimized formulas for the gravitational field of a tesseroid. *J. Geodesy*, **87**, 645–660

Heck B. and Seitz K., 2007. A comparison of the tesseroid, prism and point-mass approaches for mass reductions in gravity field modelling. *J. Geodesy*, **81**, 121–136

Hirt C. and Rexer M., 2015. Earth2014: 1 arc-min shape, topography, bedrock and ice-sheet models–available as gridded data and degree-10,800 spherical harmonics. *Int. J. Appl. Earth Obs. Geoinf.*, **39**, 103–112

Ku C.C., 1977. A direct computation of gravity and magnetic anomalies caused by 2- and 3-dimensional bodies of arbitrary shape and arbitrary magnetic polarization by equivalent-point method and a simplified cubic spline. *Geophysics*, **42**, 610–622

Kuhn M. Featherstone W.E. and Kirby J.F., 2009. Complete spherical Bouguer gravity anomalies over Australia[J]. *Aust. J. Earth Sci.*, **56**, 213–223

Laske G., Masters G., Ma Z. and Pasyanos M., 2013. Update on CRUST1.0 - A 1-degree global model of Earth's crust. *Geophysical Research Abstracts*, **15**, EGU2013-2658

Li X. and Chouteau M., 1998. Three-dimensional gravity modeling in all space. *Surv. Geophys.*, **19**, 339–368

Li Z., Hao T., Xu Y. and Xu Y., 2011. An efficient and adaptive approach for modeling gravity effects in spherical coordinates. *J. Appl. Geophys.*, **73**, 221–231

Lin M. and Denker H., 2019. On the computation of gravitational effects for tesseroids with constant and linearly varying density. *J. Geodesy*, **93**, 723–747

Marotta A.M. and Barzaghi R., 2017. A new methodology to compute the gravitational contribution of a spherical tesseroid based on the analytical solution of a sector of a spherical zonal band. *J. Geodesy*, **91**, 1207–1224

Marotta A.M., Seitz K., Barzaghi R., Grombein T. and Heck B., 2019. Comparison of two different approaches for computing the gravitational effect of a tesseroid. *Stud. Geophys. Geod.*, **63**, 321–344

Nagy D., Papp G. and Benedek J., 2000. The gravitational potential and its derivatives for the prism. *J. Geodesy*, **74**, 552–560

Nagy D., Papp G. and Benedek J., 2002. Corrections to "The gravitational potential and its derivatives for the prism". *J. Geodesy*, **76**, 475–475

Novák P. and Grafarend E.W., 2005. Ellipsoidal representation of the topographical potential and its vertical gradient. *J. Geodesy*, **78**, 691–706

Roussel C., Verdun J., Cali, J. and Masson F., 2015. Complete gravity field of an ellipsoidal prism by Gauss-Legendre quadrature. *Geophys. J. Int.*, **203**, 2220–2236, DOI: 10.1093/gji/ggv438

Shen W.B. and Deng X.L., 2016. Evaluation of the fourth order tesseroid formula and new combination approach to precisely determine gravitational potential. *Stud. Geophys. Geod.*, **60**, 583–607

Smith D.A., Robertson D.S. and Milbert D.G., 2001. Gravitational attraction of local crustal masses in spherical coordinates. *J. Geodesy*, **74**, 783–795, DOI: 10.1007/s001900000142

Tsoulis D., Novák P. and Kadlec M., 2009. Evaluation of precise terrain effects using high-resolution digital elevation models. *J. Geophys. Res.-Solid Earth*, **114**, B02404, DOI: 10.1029/2008JB005639

Uieda L., Barbosa V.C. and Braitenberg C., 2016. Tesseroids: Forward-modeling gravitational fields in spherical coordinates. *Geophysics*, **81**, F41–F48

von Frese R.R., Hinze W.J., Braile L.W. and Luca A.J., 1981. Spherical-Earth gravity and magnetic anomaly modeling by Gauss-Legendre quadrature integration. *J. Geophys.*, **49**, 234–242

Wild-Pfeiffer F., 2008. A comparison of different mass elements for use in gravity gradiometry. *J. Geodesy*, **82**, 637–653

Yang M., Hirt C. and Pail R., 2020. TGF: A new MATLAB-based software for terrain-related gravity field calculations. *Remote Sens.*, **12**, ArtNo. 1063, DOI: 10.3390/rs12071063

Zhong Y., Ren Z., Chen C., Chen H., Yang Z. and Guo Z., 2019. A new method for gravity modeling using tesseroids and 2D Gauss-Legendre quadrature rule. *J. Appl. Geophys.*, **164**, 53–64